ESI: Electronic Supporting Information

High yield detritylation of surface-attached nucleoside with photoacid generated in an overlying solid film: roles of translational diffusion and scavenging

Peter B. Garland and Pawel J. Serafinowski

E-mail: peter@garland.org.uk Pawel.Serafinowski@icr.ac.uk

NOTE: Figures, Schemes or Tables in this Supporting Information are labelled alphabetically, to avoid confusion when referring to numerical labelling in the article.

Experimental

Diffusion of TCA in films and calculation of diffusion coefficients. Experimental data were obtained as in Fig. 3 in which photoacid-induced loss of the 640 nm absorption peak of intrafilm BG slowly recovered following cessation of illumination. Film thickness was adjusted to ensure that where possible recovery rates were measurable. The thinnest films were ca. 70 nm, the thickest ca. 1.5 μm Recovery rates were equated with acid loss, an assumption that is approximate but not unreasonable when the acid and indicator have similar pK_a values, as is the case for TCA and BG. Estimates of *D*, the diffusion coefficient for TCA, were made by comparing experimental recovery curves with computer generated simulations. This gives approximate values, but is nevertheless able to compare diffusion coefficients that differed by factors from 10 to 1000-fold.

Measurement of DMT^+ removal by scavengers. Measurements in solution were made at 20–23 °C in a stoppered and magnetically stirred spectrophotometer cuvette containing 5–10 μM DMT-T, 30–40 mM TCA and according to reactivity 0.075–250 mM scavenger in a final volume of 2.7–2.8 mL. Concentrations of silane-based polymers were calculated as those of the silylhydride groups. Scavenger concentrations were in excess of those for DMT-T. The scavenger-dependent disappearance of DMT^+ measured at 503 nm followed first order kinetics after an initial lag of ca. 5 s, presumably due to continuation of acid-induced detritylation before DMT^+ removal by scavenging dominated.

Measurements in solid films for selected scavengers were made as follows. Films, 1 to 1.5 μm thick, were cast from DCM solutions containing DMT-T, PMS, ester **2**, and one of triphenylsilane (TPS), (4-methoxyphenyl)-diphenylsilane (MMPS), or triphenyltinhydride (TPTH) at wt ratios for PMS:ester **2**:scavenger of 1:1:1 for the first two scavengers and 1:2:0.1 for the third. Ester **2** was in a 40-fold molar excess over DMT-T. Measurements of DMT^+ absorption started immediately after photolysis of ester **2** at 365 nm (160 mJ cm^{-2} in 5 s). In the case of poly-(carbomethylsilane) which is both a film-forming polymer and a hydride donor, the film was cast from a DCM solution containing the polymer (1.2% w/v), ester **2** (0.3% w/v) DMT-T (0.24 mM), with or without TPM (0.17% w/v). Measurements of DMT^+ removal were made at 510 nm following rapid initial generation of TCA (and thence DMT^+) by illumination at 365 nm for 10 s (160 mJ cm^{-2}). Concentrations of scavengers in films were calculated from their relative contributions to the concentration of solutes in the film-casting solutions, and published densities (g cm^{-3}) of solutes when solid.

Detritylation equilibrium

Equilibrium concentrations for detritylation. The detritylation reaction writing ion pairs rather than single ions, total acid as a Brønsted acid HA in place of protons, and "Oligo" for "Oligonucleotide" is:

$$\text{DMT-Oligo} + \text{HA} \leftrightarrow \text{DMT}^+\text{A}^- + \text{HO-Oligo} \qquad (1)$$

The equilibrium constant *Keq* is given by

$$K_{eq} = \frac{[\text{HO-Oligo}]\,[\text{DMT}^+\,\text{A}^-]}{[\text{DMT-Oligo}]\,[\text{HA}]} \qquad (2)$$

Values of K_{eq} used in equation 2 are apparent values, varying with the strength of the acid HA. The concentrations and assigned variables or constants for the reactant concentrations at equilibrium are:

[Total Acid] = [HA] = *H*
[Total-Oligo] = [DMT-Oligo] + [HO-Oligo] = *T*
$[\text{DMT}^+\text{A}^-]$ = [HO-Oligo] = *x*
[DMT-Oligo] = *T* - *x*
Keq = *K*

Setting the acid concentration as a constant is valid for acids present in many-fold excess over DMT-oligonucleotide. Substitution of the above concentrations into equation 2 and rearrangement yields:

$$K = x^2/\{(T - x)H\}$$

which on further rearrangement gives

$$x^2 + KHx - KHT = 0 \qquad (3)$$

Equation 3 is a quadratic of the form $ax^2 + bx + c = 0$, where the values of coefficients a and b, and constant *c*, are $a = 1$, $b = KH$ and $c = -KHT$. It can be solved for x using defined values for K, H and T and the quadratic formula (equation 4):

$$x = -\frac{b \pm \sqrt{(b^2 - 4ac)}}{2a} \quad (4)$$

If the concentration of DMT^+ involved in a detritylation reaction at equilibrium were to be lowered by diffusion or scavenging, further detritylation would occur to restore the equilibrium. The new equilibrium concentrations established in response to lowering the DMT^+ concentration by an amount *delta* are given by equation 5

$$K_{eq} = \{x(x\text{-}delta)\}/\{(T\text{-}x)H\} \quad (5)$$

where
$x = [HO\text{-}Oligo]$
$(x - delta) = [DMT^+]$
$T = [HO\text{-}Oligo] + [DMT\text{-}Oligo]$
$H = [HA]$
$K = K_{eq}$

Equation 5 can be rearranged in quadratic form

$$x^2 + (KH - delta)x - KHT = 0 \quad (6)$$

and then solved for x using equation 4.

Computer simulations

Translational diffusion in films. All simulations were performed on a personal computer running Transera HTBasic[1] version 9.0 under Microsoft Windows XP or Vista. Data were exported as text files to Microsoft Excel for subsequent handling. In all cases of ionic species we have regarded their diffusion as being electroneutral even if co-diffusing or counter-diffusing ions are not specified.

Translational diffusion[2] was modelled as a series of small jumps of mean distance ± *d* (nm), constant frequency and duration per jump of *t* (s). The probability that a molecule will jump in either one of the two directions available in unrestricted one-dimensional diffusion is 0.5. Under these conditions the diffusion coefficient *D* ($nm^2\ s^{-1}$) is given by[3]

$$D = \langle d^2 \rangle / 2t \quad (7)$$

We assumed that diffusion of small molecules in the polymer film is isotropic. This might not be so if the polymer molecules have a common orientation, as could happen with flow of a viscous casting solution of a polymer of high molecular weight and linear structure, but these conditions did not apply: we used polymers of mol wt < 3,000 in dilute non-viscous solution.

As shown in the Scheme there are three axes available for diffusion: the *x*- and *y*-axes in the plane of the film, and the *z*-axis orthogonal to it. The oligonucleotide layer forms a thin compartment chemically different from, but still within, the thicker film of polymer and photoacid generator.

Photoacid generation was assumed to be effectively instantaneous on the time scale of diffusion in a polymer. We also assumed that the concentration of photoacid is initially uniform throughout the whole film. The glass slide supporting the film provides an impermeable barrier to diffusion, reflecting back any molecules that collide with it. The film/air interface is also regarded as impermeable except to volatile compounds such as TCA. Oligonucleotides, tritylated or not, are covalently attached to the glass surface and cannot diffuse.

The diffusional movements of interest are those of DMT^+, HA, H^+, A^- and the ion pairs H^+A^- and DMT^+A^- that may be formed in an aprotic environment. We assumed that all diffusion is electroneutral, either as uncharged compounds (e.g. HA) or ion pairs (DMT^+ with A^-), or by exchange (e.g. DMT^+ with H^+).

Scheme 3-Dimensional photoacid generating film with an oligonucleotide layer on a support.

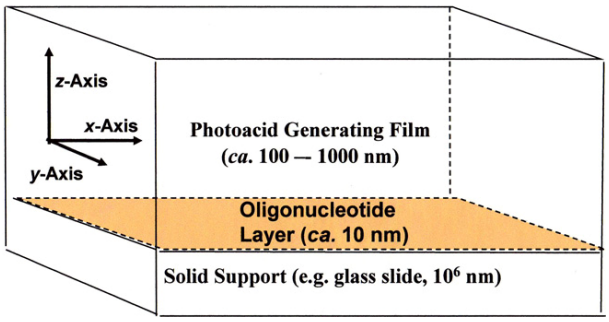

We also assumed that the polymer does not bind other molecules, and provides an inert environment that restricts diffusion. The mechanism of diffusion in polymers is thought to involve thermally activated movements of polymer segments that temporarily open small spaces into which an adjacent small molecule can jump. Factors that increase intrafilm diffusion rates of small molecules include increased temperature, polymer structures that pack less closely, and the incorporation of small molecules, so-called plasticizers, that disrupt tight packing of the polymer.

Four physical arrangements were relevant to our experimental studies: (i) diffusion of TCA in the z-axis and its loss from the film at the film/air interface (ii) diffusion of TCA in the plane of the film of the plane normal to a straight boundary between illuminated (photoacid present) and non-illuminated (photoacid absent) film areas: i.e.

(1) Transera Corp., Orem, Utah, USA. (www.htbasic.com)
(2) From now on referred to simply as "diffusion"
(3)P.R Bergethon, E.R Simons,- *Biophysical Chemistry* (Springer-Verlag, Berlin), **1989,** 233–234.

diffusion along intrafilm x- or y- axes (iii) diffusion of DMT^+ in the *z*-axis, moving from the oligonucleotide layer into the overlying film volume, and (iv) kinetics of the reaction between a carbocation scavenging reagent and DMT^+ within the film.

Simulation of z-axis diffusion of TCA with loss at the air/film interface. The film was modelled as being 100 nm thick, divided into 100 layers of 1 nm each equal to the jump distance of 1 nm. It is assumed that (a) movement of TCA from the film surface into the air phase, although in principle reversible, is in effect irreversible due to the large volume of air, and (b) acid attempting to diffuse into the glass support from the contacted layer is reflected back. For all other layers the probabilities that an acid molecule jumps into the adjacent layer (n – 1) or (n + 1) are 0.5 for each. The simulation commences at zero time with the acid concentration in each layer being set at 1.0 arbitrary units, as would be the case following a brief photogeneration of acid in the absence of any inner filter effects. A reiterative loop calculates the new acid concentration in each layer after each of many diffusional jumps. Except for the two interface layers (support/film and film/air) the value in each *n*th layer is the sum of half the immediately previous values in the adjacent layers *n+1* and *n-1*. The value for the layer at the film/air interface is given by half the value in the preceding layer. The value at layer $n = 0$ at the interface with the underlying support is given by the sum of half the previous values for layer $n = 0$ and $n = 1$.

Fig. A shows the *z*-axis distribution of acid concentration for a range of diffusional jump numbers from 0 to 24,300. As expected the acid concentration falls most rapidly in the layers closest to the film/air interface, and more slowly in the deeper layers.

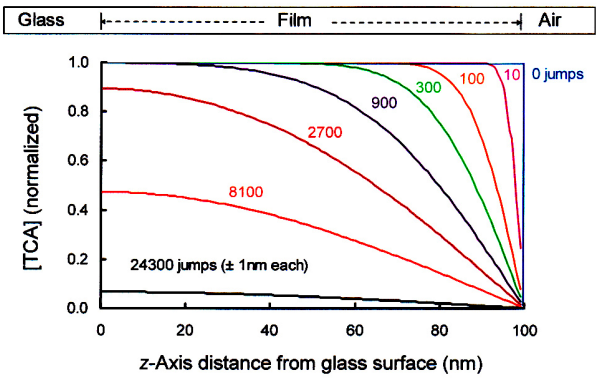

Fig. A. Diffusional loss of a volatile acid from a 100nm thick solid film by *z*-axis diffusion. The plots are for the acid concentration profile along the *z*-axis extending from the glass/film to film/air interfaces after 0, 10, 100, 300, 900, 2700, 8100 and 24300 diffusional jumps of ± 1 nm each.

Fig. B uses data obtained in Fig. A to show the decay of the mean intrafilm acid concentration as diffusion progresses.

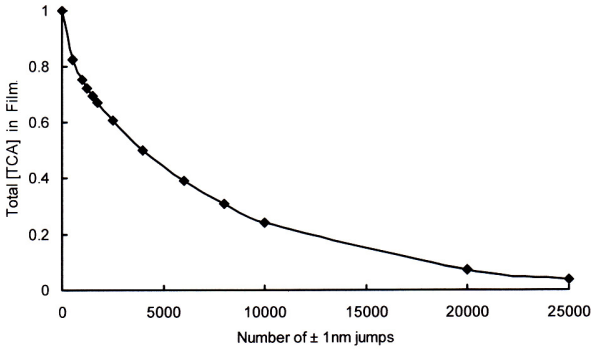

Fig. B Decay of mean intrafilm acid concentration with increasing number of diffusional jumps in the z-axis. Each point is the mean acid concentration value for a profile obtained as in Fig. A.

When the jump number in Figure B is multiplied by the jump period *t* the graph becomes a time-dependent decay curve for acid concentration. The value of *t* can be adjusted to give a decay curve with a half-life matching that for the experimentally observed recovery of BG absorption at 640 nm in response to falling intrafilm acidity (Article, Fig. 4). The value of D is then calculated from equation 7 using *H/100* for the jump length *d* where *H* is the experimentally determined film thickness, and *t* the best fit value for the duration of one jump.

Simulation of acid diffusion in the x- or y-axis. A diffusional jump model is again used. It is assumed that the film is sufficiently thick to ignore loss of acid at the air/film interface. The model is for the concentration profile of acid along an axis in the plane of the film and orthogonal to the boundary between an illuminated and adjacent non-illuminated area. It differs from the model for z-axis diffusion in that (a) diffusion is in the plane of the film (b) the many layers each the thickness of 1 diffusional jump are perpendicular to the plane of the film, and (c) the two ends of the profile are sufficiently far from the boundary between the illuminated and non-illuminated areas for their acid concentrations to remain as 1.0 and zero respectively despite diffusion. The initial acid concentrations immediately following photogeneration are normalized as 1.0 for all sections in the illuminated area and zero for those in the non-illuminated area. Diffusion then proceeds by a series of regular jumps of mean length ± *d* nm and duration *t* s. New values for acid concentrations in each layer are recalculated after each jump. Fig. C shows the outcome for a range of jump numbers.

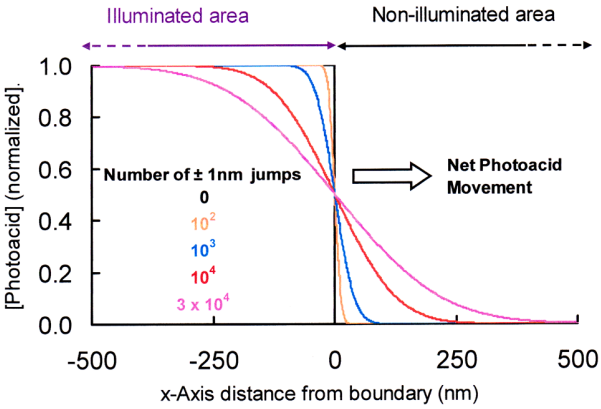

Fig. C Diffusion of photoacid in the *x*-axis from an illuminated to non-illuminated film area. The simulation shows intrafilm concentration profiles of photoacid across the interface. The jump distance was ± 1 nm. No account has been taken of the effects of light diffusion at the edge on the zero-time profile.

The data of Fig. C provide guidelines for acceptable diffusion coefficient values for a given photolithographic resolution. For example, 10^4 jumps would not extend the boundary of diffusing photoacid more than 250 nm from the boundary between illuminated and non-illuminated areas. A total of 10^4 diffusional jumps each ± 1 nm and occurring after photoacid generation (modelled as instantaneous) over 50 s corresponds to D = 100 $nm^2\ s^{-1}$ (equation 7). This increase of photoacid diffusion would not cause unacceptable loss of photolithographic resolution for array elements > 4 x 4 μm. The sigmoidal dependence of detritylation on photoacid concentration observed with ester **2** provides further protection against loss of photolithographic diffusion. Additional protection can be obtained by inclusion of a low concentration of base within the film.

Simulation of DMT^+ diffusion in the z-axis. The model involves (a) instantaneous equilibration of a thin layer of surface-attached DMT-oligonucleotide with photoacid generated in an overlying photoacid-generating film (b) diffusional movement of released DMT^+ along the *z*-axis, away from its site of release (c) reflection back into the film of any DMT^+ attempting to leave the film at either the film/air or film/support interfaces (d) readjustment of the detritylation equilibrium position in response to movement of DMT^+ away from the surface layer of attached oligonucleotide. As with the simulations already described above, diffusion is modelled as repetitive jumps at constant frequency and a mean distance of ± 1 nm per jump throughout a film thickness composed of up to several hundred consecutive 1 nm layers.

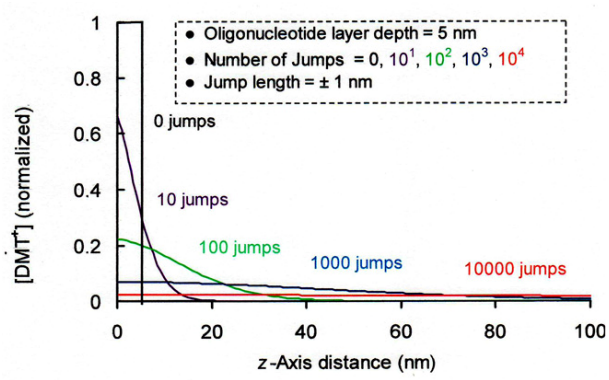

Fig. D Diffusion of DMT^+ in the z-axis. Oligonucleotide is confined to a 5 nm thick zone at the surface of the film-supporting glass. The diffusional jumps are commenced immediately following acid induced detritylation. The latter is modelled as instantaneous and complete.

Adjustment of the detritylation equilibrium position to diffusional loss of DMT^+ from the oligonucleotide layer was made at the end of each round of jumps. This can be done by use of equation 6. Alternatively a numerical method can be used wherein [Oligo-OH] is adjusted by very small increments of further detritylation until the calculated value of *Keq* equals the defined one. An example is given at Fig. 2 of the Article. Fig. D shows an example where the initial detritylation is 100%, and re-equilibration of the detritylation reaction is not required.

Simulation of diffusional replacement of photoacid consumed in detritylation of oligonucleotides at the film/glass interface. The surface density of DMT-T used in our experiments was 5- to 18- fold higher than the 40 pmol cm^{-2} typically used for oligonucleotide arrays. The depth of the oligonucleotide layer will depend on the length and area density of the oligonucleotides, but for illustrative purposes we assume a value of 10 nm. The issue then is whether the concentration of photoacid in that layer is significantly lowered by consumption in the detritylation reaction, such that further acid must diffuse into the layer from the overlying film to maximise detritylation.

Film concentrations of photoacid can be calculated from measurements of its area density and film thickness. In the experiment shown in Fig. 5 of the Article, the area density of photogenerated TCA was ca. 15,000 pmol cm^{-2}, well in excess of the initial DMT-T density of 400 pmol cm^{-2} for prior to illumination. But the TCA is distributed throughout the whole 220 nm thickness of the film, so the amount in the 10 nm layer of surface-attached DMT-T is only 1/22 of the total, or 680 pmol cm^{-2}. In which case detritylation, being reversible, would be limited by falling TCA concentrations unless they are recovered by diffusion from the overlying film.

How fast might diffusional recovery be? Fig. E shows recovery curves for the simple case of a thought experiment where acid in the 10 nm thick layer of film at the glass

surface layer is suddenly reduced to zero, and is then replenished by *z*-axis diffusion of acid from the much thicker overlying layer. The time scale for diffusion of acid from the overlying film into the surface-attached oligonucleotide layer is very similar to that for DMT^+ movement in the opposite direction, shown in Figure D.

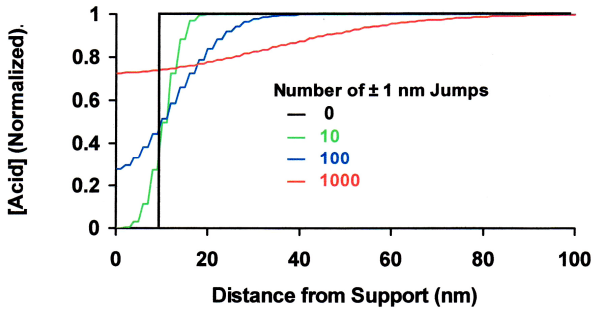

Figure E Recovery from acid depletion in a 10 nm thick layer of surface-attached nucleotide. The simulation commences with no acid in the first 10 nm of a 100 nm thick film contacted to a planar surface. The remainder of the film contains acid evenly distributed at a normalized concentration of 1.0. Diffusion in the z-axis normal to the plane of the film with jumps of ± 1 nm.

Simulation of decay of a striped photoacid pattern. Fig. 4 of the Article showed a microphotograph of alternating green and white stripes observed in a film of photoacid-generator containing the pH indicator BG, after photolysis through a contacted Rhonchi ruling. The line width for the ruling was 10 µm. The effects of *x*-Axis diffusion on decay of a striped photoacid pattern are shown in Fig. F. Simulation was made for three consecutive dark/light boundaries.

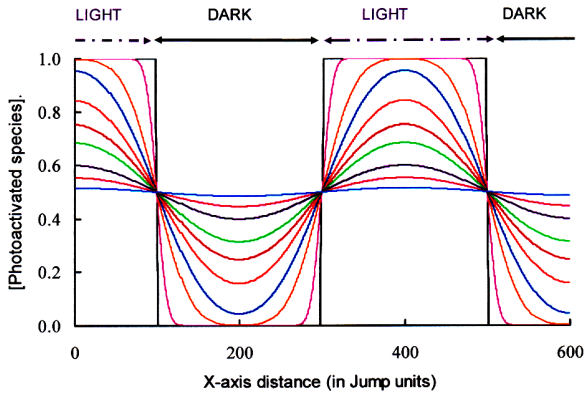

Figure F. Concentration profiles following patterned photoactivation of a light-sensitive film component using illumination through a Rhonchi ruling. The arrows at the top indicate illuminated and non-illuminated areas. Photoactivation is instantaneous, and the resulting concentration profile of photoactivated species along an axis in the plane of the film and orthogonal to the rulings is a square wave. The x-axis is scaled in units equal to the length of one diffusional jump, and extends from the centre of a transparent line at the left for 1.5 periods to the centre of an opaque line at the right. The line width is 200 jump units, and concentration profiles are shown for a range of jump units. The figure can be scaled to any Rhonchi ruling by defining the jump unit length and to any diffusion coefficient or time by defining one and calculating the other from equation 7. Jump numbers for the individual plots are **0**, 10^2, 10^3, 2.5×10^3, 5×10^3, 7.5×10^3, 10^4, 1.5×10^4, 2×10^4 and 3×10^4.

The jump length for this model with 10 µm wide stripes is 20 nm, and for D = 50 nm^2 s^{-1} the duration of each jump given by equation 7 is 25 s. Decay of the pattern by diffusion is therefore slow, over many hours.

Kinetics of DMT^+ scavenging

Computer simulations. The detritylation reaction was maintained at equilibrium. Deviation from equilibrium, such as that caused by DMT^+ scavenging or diffusion out of the layer of attached oligonucleotide into the overlying film, was corrected by calculation of a new equilibrium position. Thus if the DMT^+ concentration was lowered, further detritylation occurred to give a new equilibrium. Concentrations of acid remained effectively constant, simplifying the calculation of equilibria. Concentrations of scavenger were also sufficiently high to remain constant, enabling DMT^+ removal to be modelled as a first order reaction.

Combining scavenging with *z*-axis diffusion of DMT^+ from the oligonucleotide layer into the overlying film was straightforward: scavenger concentration was effectively constant throughout the film, and each of the many 1 nm layers used for the repetitive diffusional jump model was subjected to recalculation of DMT^+ concentration due to scavenging occurring during each jump period.

These calculations for DMT^+ diffusion and removal by scavenging extended over all layers of the film. Re-adjustments of the detritylation equilibrium applied only to those layers containing oligonucleotide. They were modelled as the first ten layers, each 1 nm thick, where the concentration of oligonucleotides, both detritylated and tritylated, was assumed to be constant. Unless acid activity is extremely high the extent of detritylation is incomplete on completion of photoacid generation, and the subsequent rates of scavenging are affected by the lower initial DMT^+ concentration and its replenishment by further detritylation. Thus the detritylation rate due to scavenging depends not only on the concentration of scavenger and its reactivity but also on the photoacid concentration. A similar consideration applies to DMT^+ diffusion, which like scavenging commences only when DMT^+ has been formed.

The effect of acid concentration on scavenging rates can be modelled most simply under circumstances where there is no DMT^+ diffusion to complicate matters by causing further detritylation. Fig. G shows the time dependence of detritylation in the presence of excess scavenger, calculated for six different acid concentrations. The calculation assumes that the detritylation reaction instantly equilibrates with acid and remains close to equilibrium throughout, so

the protracted time-dependent detritylation phase is due to scavenging of DMT^+.

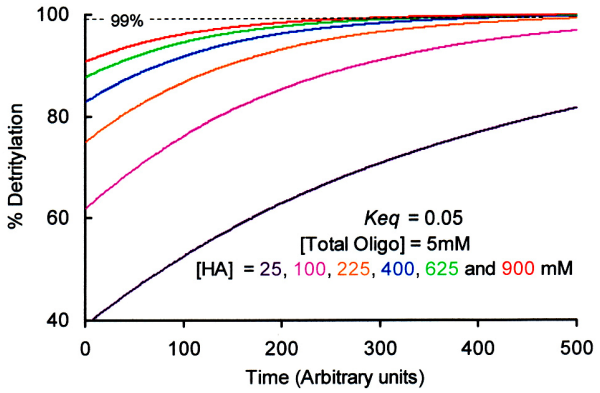

Fig. G Calculated effects of acid concentration on the time-dependent effects of scavenging on the extent of detritylation, in the presence of excess scavenger. The concentrations of acid (HA) are as shown. K_{eq} for detritylation = 0.05. [DMT-oligo] prior to detritylation = 5 mM. At each successive time unit other than the first (i.e. Time = 0) the equilibrium of the detritylation reaction was recalculated after lowering the value of $[DMT^+]$ by a factor f = (1 - k') where k' is the pseudo first-order rate constant corrected for the arbitrary time unit in use. Thus if each time unit is 0.1 s and the rate constant k = 0.01 s^{-1} then k' = 0.001, the factor f = 0.999, and the time scale is from 0 to 50 s. The horizontal interrupted line is at 99% detritylation.

The time scale and scavenging rate constant used for Fig. G are applicable to experimental conditions using (4-methoxyphenyl)-diphenylsilane (MMPS), or triphenyl-tinhydride (TPTH) in solid films of poly(α-methylstyrene), ester **2** and DMT-T (Fig. 6 of the Article). More rapid scavenging is required when the pre-scavenging extent is low, as with lower acid activities, and would be achievable using tripenyltinhydride.

Diffusion and film composition

Choice of film-forming material. The rates of diffusion of small molecules within a solid film can be varied by choice of the film-forming material, typically but not necessarily a polymer, or by inclusion of so-called plasticizers in the film. Examples of the effects of film composition on intrafilm diffusion, detritylation and scavenging rates are given in the Results Section of the Article.

Where polymer preparations were available over a range of molecular weights we chose those at the lower end of the scale, < 10 kDa, in anticipation that intrafilm diffusion would be faster than with films of higher molecular weights.

The glass transition temperature (T_g) of polymers is also a possible indicator of their relative constraints on intrafilm diffusion of small molecules. Below T_g the polymer molecules are in a more ordered arrangement with low segmental motion, resulting in a hard and more brittle solid. Above T_g the polymer molecules are less ordered and in a more amorphous state. The solid is softer, more flexible, and with increased segmental motion that allows faster intrafilm diffusion. Polymers such as polybutadiene or copolymers thereof containing *cis* ($–CH_2CH=CHCH_2–$) subunits have lowered melting points and maybe liquids at molecular weight values (e.g. 5,000) where most other hydrocarbon polymers are solids. The *cis*-configuration results in poor packing of polymer chains, increased chain mobility and lowered melting points. Inclusion of *cis*-butadiene or poly(*cis*-butadiene) in *co*- or *block*- polymers with styrene or polystyrene polymers converts these hard polymers into thermoplastic forms. This approach is an alternative to adding low molecular plasticizers.

Using the method described in the Article (Experimental and Fig. 3) we compared the rates of TCA diffusion in films containing poly(α-methylstyrene) or polystyrene-*block*-polybutadiene-*block*-polystyrene (mw ca. 140,000. styrene content 30%) at a 5:1 weight ratio to the photoacid generator ester **2**. The diffusion coefficient in the film of polymethylstyrene was < 0.1 nm^2 s^{-1} and in the other ca. 300 nm^2 s^{-1}).

But although thermoplastic polymers offer a route to adjusting intrafilm diffusion rates, there are three factors not in their favor: (i) presence of alkene subunits risks unwanted chemical reaction during photolysis or DMT^+ carbocation generation (ii) adjustment of diffusion rates by change of polymer composition is at best cumbersome (iii) the risk of microphase separation of *block*-polymer domains, resulting in non-uniform intrafilm conditions.[4] These drawbacks are avoided with incorporated plasticizers in films of non-thermoplastic polymers.

Plasticizers. Commonly used and commercially available plasticizers contain oxygen, typically in ester groups, and are therefore likely to cause weakening of carboxylic acids by hydrogen bonding. As an alternative we explored a set of solid aromatic hydrocarbons. Some of these compounds can be regarded as oligomers.[5] Our criteria for initial selection included lack of electronegative heteroatoms, melting point above ambient temperature, commercial availability, low cost, chemical stability, and anticipated solubility in DCM based on high content of aryl groups and low content of alkyl groups unless short chain. We tested the compounds listed below (Table A). All were

(4) M.J Fasolker, L. S. Goldner, J. Hwang, A. M. Urbas, P. DeRege, T. Swager, E. L. Thomas, *Phys. Rev. Lett*. **2003**, *90*, 016107-1 to 016107-4.

(5) M Rothe, in *Polymer Handbook*, 4th Ed., J. Branderup, E.H. Immergut, E. A. Grulke, Eds., J. Wiley & Sons Inc, Chichester, **1999**, Section IV, 1–93 "Physical data of oligomers".

soluble in DCM at 2% (w/v), though the rate of dissolution varied. When cast from solution on a microscope slide, triphenylmethane formed an optically clear and solid but soft film. 1,4-Bis(2-methylstyryl)benzene formed a hard, clear film with crazing, whereas the remainder gave irregular deposits.

When poly(*α*-methylstyrene) films were made with inclusion of the selected members *(italicised)* from Table A there were differences in their feel on being touched. Softness and tackiness are both indicators of greater intrafilm disorder, and although subjective and qualitative, they nevertheless provide a quick and simple test. The lower molecular weight plasticizers such as biphenyl, bibenzyl or 4-phenyltoluene were more effective, on a weight basis, in increasing tackiness and softness of poly(*α*-methylstyrene) films than the others.

Effects of plasticizers on diffusion of TCA in films of poly(*α*-methylstyrene). We again used the method described in the Article, but with thicker films (ca. 0.5 μm) to accommodate the faster diffusion rates. We tested bibenzyl, 4-phenyltoluene and triphenylmethane each at 1:1:1 w/w ratios with poly(*α*-methylstyrene) and photoacid generator (ester **2**) in films containing the pH indicator BG spread on slides. Diffusional loss of TCA following its photogeneration from ester **2** was equated with reappearance of the 640 nm peak of non-protonated BG following its virtual disappearance on photoacid generation. These relatively slow post-photolysis changes over several minutes were not observed in the absence of the plasticizers: the estimated diffusion coefficients in their presence were *ca.* 100-200 $nm^2\ s^{-1}$. These may be higher than would be used in practice for very high density photodirected oligonucleotide array fabrication, and can be lowered by reducing the plasticizer concentration.

Table A. Some possible film plasticizers that lack electronegative heteroatoms. Those listed *in italics* could be incorporated in film-casting solutions of poly(*α*-methylstyrene) at ratio of polymer : plasticizer of 2 : 1 by weight without disruption of subsequent film formation.

Compound	mp (°C)	mol wt (Da)
4-Benzyl(biphenyl)	85–87	244
Bibenzyl	69–72	182
Biphenyl	69–72	154
1,4-Bis(2-methylstyryl)benzene		310
2, 3 Dibenzyl-1,3-butadiene	86–88	234
4,4'-Dimethylbiphenyl	119	182
Hexamethylbenzene	166–168	162
2-Phenylindene	157–161	192
4-Phenyltoluene	44–47	168
1,2,4.5-Tetramethylbenzene	81	134
1,1,4,4-Tetraphenyl-1,3-butadiene	197	358
1,2,3,4-Tetraphenyl-1,3-cyclo-pentadiene	180–182	370
Tetraphenylethylene	222	332
1,3,5-Triphenylbenzene	172–174	306
Triphenylethylene	70	256
Triphenylmethane	92	*244*

End of ESI